

Influence of the Interpass Welding Temperature on Microstructure and Corrosion Resistance of Superduplex Stainless Steel SAF 2507

Frederico Augusto Araújo Macedo^{a*}, José Adilson de Castro^{a*} , Claudinei dos Santos^{a,b} ,
Kurt Strecker^c , Carlos Roberto Xavier^d 

^aUniversidade Federal Fluminense, Escola de Engenharia Industrial Metalúrgica de Volta Redonda, Volta Redonda, RJ, Brasil

^bUniversidade do Estado do Rio de Janeiro, Faculdade de Tecnologia de Resende, Resende, RJ, Brasil

^cUniversidade Federal de São João Del'Rei, São João Del-Rei, MG, Brasil

^dCentro Universitário de Volta Redonda, Volta Redonda, RJ, Brasil

Received: June 1, 2020; Revised: March 21, 2021; Accepted: April 6, 2021

The planning and execution of the adequate welding procedure for the superduplex stainless steel (SAF 2507 SDSS) in multiple passes is a complex technological task since thermal cycling may cause the precipitation of harmful phases, such as the sigma (σ) and chi (χ) phases. For this reason, technical standards limit the maximum interpass temperature (T.I.) in an extremely conservative manner at 100 °C. In order to investigate a possibly wider temperature range for this procedure, SAF 2507-SDSS tubes were subjected to autogenous Tungsten Inert Gas (TIG) welding with interpass temperatures ranging from 150°C to 400°C. The different welding zones were characterized by microscopy, Vickers microhardness, and polarization corrosion tests. The results indicated that in the Fusion Zone (FZ), columnar grains of ferrite were formed surrounded by allotriomorphic austenite (AA), besides intragranular austenite (AI) and Widmanstätten austenite (AW). The heat-affected zone (HAZ) had a lower ferrite content and was composed of equiaxed grains of ferrite, also surrounded by AA, besides AI and AW. Hardnesses varied between HV272 and HV293, regardless of the region or the interpass temperature used. Furthermore, the corrosion resistance has not been significantly affected by the interpass temperatures between 150 °C and 400°C.

Keywords: SAF 2507 SDSS, Tungsten Inert Gas (TIG) welding, interpass temperature, microstructure, corrosion resistance.

1. Introduction

The study of welded joints of the SAF-2507 SDSS superduplex stainless steel is of great importance, as it is a material of high applicability. These steels are widely used in the oil, naval, and paper industries, among others^{1,2}. The superduplex stainless steels are notable due to their high mechanical strength and excellent corrosion resistance. These characteristics are attributed to the presence in equal proportions of ferrite and austenite with considerable amounts of chromium and nickel in their composition, besides favorable grain boundary morphologies. The welding procedures usually designed for SAF-2507 SDSS is considered delicate because during thermal cycling of these materials, the phase composition may become unbalanced or the precipitation of secondary phases, such as nitrides, carbides, (σ) and chi (χ) phases, may occur, causing a significant loss of mechanical strength and corrosion resistance. It has been reported that the precipitation of only 4% of these undesirable phases can reduce the toughness of steel by up to 90%^{3,4}.

SAF-2507 SDSS has a low thermal expansion coefficient and a thermal conductivity superior to common austenitic stainless steels. These superduplex stainless steels are applied

under extremely aggressive situations where the deterioration of properties is critical. Thus, the recommended heat input is limited to the range of 0.2 - 1.5 kJ.mm⁻¹ in the welding processes of this kind of steel⁵⁻⁹. The TIG process applied under controlled conditions presents advantages such as the absence of spatter, a good aspect of the weld bead, besides the possibility to weld also thin parts^{2,10}. Shielding gases such as argon, helium, the combination of both in variable proportions and a small amount of nitrogen are commonly used. They can help to obtain the adequate austenite-ferrite phase balance^{11,12}. Autogenous soldering is a process in which metal parts are joined without solder, i.e. the electric arc formed by the electrode fuses the parts allowing the joint consolidation without using consumable materials and hence have an important impact on fabrication cost and energy consumption. However, this procedure requires a strict control of the local thermal state in order to compensate for the usual benefits obtained by adding alloying elements through the consumable materials.

According to the Norwegian standard NORSOK M-601¹³, a widely accepted reference in the standardization of this type of welding processes, the maximum interpass temperature in materials of the super duplex classes should not exceed

*e-mail: joseadilsoncastro@id.uff.br

100 °C, i.e., for a second pass to be made, one must wait until this temperature is reached in the weld joint, leading to a reduction in the productivity and an increased cost of this manufacturing process. Several researchers have studied the mechanical properties, microstructural aspects, and corrosion resistance of the SAF 2507 SDSS^{11,13-15}. Nevertheless, investigations connecting the welding conditions to the microstructure, mechanical properties and corrosion resistance to establish a broader standard for the tube welding by the TIG process are scarce and deserve further studies.

The current work aims to demonstrate the adequacy of a two pass TIG autogenous welding process for SAF 2507 SDSS, using interpass temperatures higher than recommended by the NORSOK M-601 standard. This study's innovative aspect is justified by the possibility of using higher Interpass welding temperatures, productivity may be improved, resulting in a lower cost of gas pipelines and refinery equipment's constructions using these high-grade materials, in contrast to competing alloys applied in this field¹³⁻¹⁵. Moreover, new technological applications such as heat exchangers, pressure vessels, and evaporators may become competitive for energy facilities by using this procedure. The viability of using higher interpass temperatures in tube welding procedures can be demonstrated by studying their influence on the microstructures, mechanical properties, in particular hardness, and corrosion resistance of SAF 2507 SDSS joints.

The use of interpass temperatures higher than those recommended by the NORSOK M-601 standard could lead to significant gains in productivity and reduction of energy consumption in the procedures currently employed. Furthermore, construction of newly designed equipment with enhanced performance to extended life may become viable. Incremental improvements in this procedure decrease the costs and enhance the knowledge for safe welding procedures for tubes made of SAF 2507 SDSS.

2. Experimental Procedure

2.1. Material

In this work, SAF 2507 SDSS tubes with an external diameter of 168 mm and 3.5 mm thickness were used. The chemical composition of the material is shown in Table 1.

2.2. TIG welding procedure

The autogenous TIG welding process (without solder) was carried out in an inverter machine for TIG AC/DC welding and coated electrodes model CastoTig 2003 AC/DC, adapted to welding automation. In this stage, the thermal input for SAF 2507 SDSS (in the range of 0.2 - 1.5 kJ.mm⁻¹) was respected, using argon as shielding gas to reproduce the welding conditions applied in joining tubes of small pipelines, typical of oil and gas processing plants.

Two pipe segments were used for the welding studies. In each segment, two different welding procedures of two passes were executed, with the interpass temperature as the only variable in each procedure. The first pass occurred at room temperature, and the welding procedure was carried out throughout the tube's circumference. In the second pass, a previously defined interpass temperature was used in each test, monitored by thermocouples, returning from the end of the first pass without completing the loop of the tube, to prevent the beginning of the cord from undergoing yet another reheating process and also to prevent the area affected by the heat-release of the first pass from being completely overlapped or destroyed by the second. For this purpose, a lower thermal input was used in the second pass than in the first pass, aiming only to reheat the area affected by the heat of the first pass before its cooling down and then evaluating the effect of this procedure.

A general view of the tube parts assembly, temperature monitoring positions and sample analysis retrieval is shown in Figure 1. Four thermocouples were positioned and used for monitoring the temperature throughout the process, as shown in Figure 1a. One placed at the end of the first pass, another at 10 mm from the end, another at 40 mm from the end, and another halfway through the return path. After completion of the first pass, welding only recommenced when the thermocouple's temperature located at the end of the first pass indicated the ideal interpass temperature for each test of 150 °C, 250 °C, or 400 °C, respectively.

TIG welding was conducted under pulsed current, with a base current of 150 A with a duration of 0.006 s and a peak current of 250 A with a duration of 0.004 s. The frequency used in the equipment's motor was 5 Hz forward and 10 Hz backward, corresponding to a forward speed of 4.10 mm.s⁻¹ and a backward speed of 8.23 mm.s⁻¹. These values were selected after calibration to ensure a uniform and stable weld bead. An argon flow of 16 L.min⁻¹ was used, and the distance between the electrode and the part was approximately 1.5 mm.

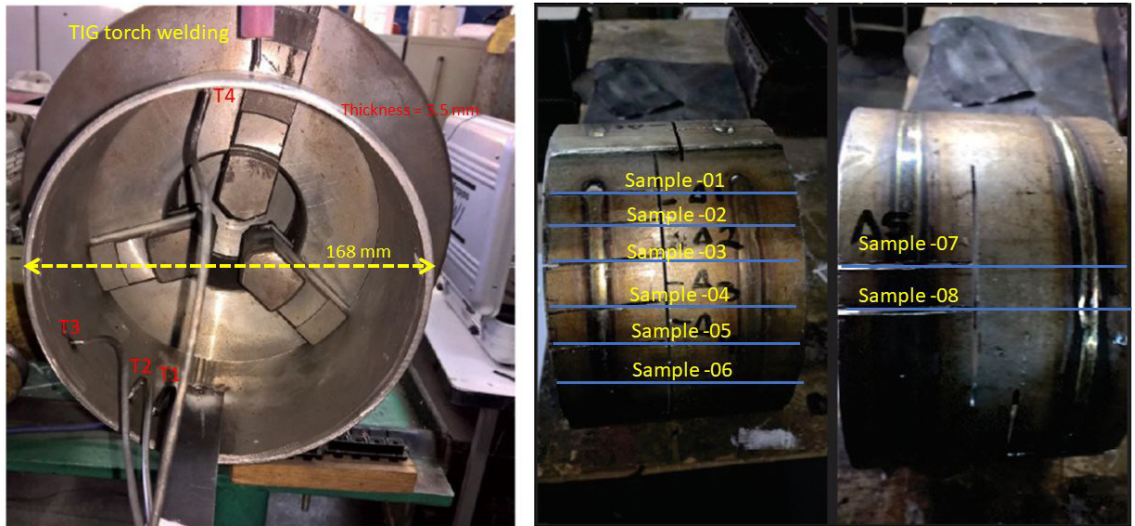
The data were collected with SAP V4 equipment, combined with the data acquisition software for welding SAP V4.19, to precisely monitor the welding process. Table 2 presents a compilation of the parameters used in the welding process.

The samples were sectioned perpendicular to the weld bead, with a width equivalent to half of the tube's height. After the cuts, the samples were identified according to the thermocouples' position and the thermal input used in welding the tube (see Figure 1b). Finally, the sample surfaces were sanded with SiC sandpaper and polished with 6, 3, and 1 µm grade diamond paste, respectively. The samples' microstructure was revealed by chemical etching with a modified Beraha solution (80 mL of distilled water, 20 mL of hydrochloric acid, 2 g of potassium sulfite, and 2 g of ammonium biftuoride) for 10 seconds. This procedure has been used in similar researches with some adjustments¹¹⁻¹⁶.

Table 1. Chemical composition of SAF 2507 – SDSS (%) (data provided by the manufacturer "Sandvik Group").

UNS*	EN**	Nomenclature	C _{max}	Cr	Ni	Mo	Mn	Si	Co	Cu	N
S32750	1.4410	SAF 2507	0.03	24-26	6.0-8.0	3.0-5.0	1.2	0.8	-	0.5	0.24-0.32

* Unified Numbering System for Metals and Alloys / ** European Standard, PREN= 42.5 (estimated pitting resistance equivalent number)



a) Assemble for automatic welding procedure and monitoring

b) Locations for samples retrieval

Figure 1. General assembly of the tube sample welding: a) Positioning of thermocouples for measuring the temperature during the TIG welding process, b) Locations of the sample's extractions.

Table 2. Parameters of the autogenous TIG welding process.

Procedure	Interpass directions and temperature	Frequency (Hz)	Velocity (mm.s ⁻¹)	Instant results			
				Current (A)	Tension (V)	yield (%)	Heat input (kJ.mm ⁻¹)
1	ahead	5	4.10	178.77	13.29	78	0.45
	150°C back	10	8.23	180.09	14.06		0.24
2	ahead	5	4.10	177.12	12.49	78	0.42
	250°C back	10	8.23	176.75	12.40		0.21
3	ahead	5	4.10	177.26	13.29	78	0.45
	400°C back	10	8.23	177.72	13.49		0.23

2.3. Characterizations

2.3.1. Microstructure

The microstructural analysis of the base metal (BM), the heat-affected zone (HAZ), and the fused zone (FZ) was done by optical microscopy (OM) and scanning electron microscopy (SEM), respectively, using an Olympus optical microscope and a Zeiss EVO MA10 scanning electron microscope equipped with an EDS system.

2.3.2. Quantitative phase analysis

The volumetric fractions of ferrite and austenite were determined using micrographs, following the ASTM E-562-19 standard¹⁷, using 16-point grids on each image to calculate the respective volume fractions. The grain thickness was measured by using the intercept method. All the measurements were repeated 20 times, and the average values calculated.

2.3.3. Mechanical characterization

Hardness was determined by the Vickers indentation method. The samples' cross-sections were subjected to Vickers hardness measurements using a DHV-1000Z-Time-corporation hardness tester, applying an indentation load of 9.81N (1000 gF). The measurements (n> 5/line) were carried out in the cross-sectional area of the samples, which involves

the heat-affected zone of high temperature (HAZHT), the heat-affected zone of low temperature (HAZLT), the base metal (MB) and the fused zone (FZ), for each of the three thermal conditions studied in this work.

2.3.4. Polarization corrosion test

Each zone identified in the sample's surfaces was exposed to an analytical solution corrosion media. The exposed areas were selected to cope with a representative surface of 200 μm² in all experimental runs. The corrosion tests were carried out in an aqueous solution containing 3.5% NaCl, room temperature, and without stirring. Analytical grade reagents and Milli-Q water (18.2 MΩ cm) were used to prepare the solutions. The polarization curves were obtained using a scanning potentiostat cell (EmStat3+, PalmSens). The anodic potential scanning started at -0.15 mV, scanning at 1 mV.s⁻¹ towards the positive potential, until localized corrosion was achieved. To ensure reproducibility, a minimum of two runs were performed for each experiment, and the averaged curve plotted to extract the characteristic corrosion currents (I_{corr} , I_{pit}) and potentials (E_{corr} , E_{pit}). A platinum wire was used as counter-electrode, and a tungsten wire covered with tungsten oxide dipped directly in the working solution was used as reference electrode. In this procedure, the corrosion potential (E_{corr}) and the pitting potential (E_{pit}) obtained after

the cyclic polarization were compared with the reference material, BM. The corrosion resistance of the material was associated with the pitting corrosion potential. To compare the materials it was assumed that the higher E_{pit} , the more corrosion resistant the material was. These values were compared to analyze the weld joints HAZ and FZ regions under the variable conditions of the interpass temperatures.

3. Results and Discussion

3.1. Microstructural characterization

Images comparing the grain morphologies of each region, FZ, HAZ, and BM, for different interpass temperatures are shown in Figure 2.

As expected, the BM consists of alternating lamellar grains of austenite in a ferritic matrix throughout the region¹¹⁻¹⁶. The FZ presents columnar grains of ferrite, oriented in the direction of heat extraction and grain boundaries formed by austenite. The heat-affected zone, HAZ, exhibits smaller and equiaxed ferrite grains, and like in the FZ, the grain boundaries are formed by austenite. Comparing the micrographs of the welded SAF 2507 SDSS tube after two passes (b, c, d) with the images after just one pass (a), it is noted that the image (a) presents a denser structure, richer in austenite in the FZ region. Figure 3 shows representative optical micrographs of the different regions of the welded SAF 2507 SDSS tube, where (a) is the base metal, (b) the heat-affected zone and (c) the fusion zone. The weld bead formed with an interpass temperature of 250 °C is typical, showing the FZ, HAZ, and the BM clearly distinct, see Figure 3b, with a transition of columnar grains from the FZ to equiaxed grains in the HAZ to lamellar grains of austenite in a ferritic matrix.

Figure 4 shows the microstructures of each zone for different interpass temperatures. In the fused zone (FZ) and the heat-affected zone (HAZ), the phases Ferrite (α) and Austenite (γ) are represented by the dark and bright phases in the micrographs, respectively. A general aspect of the micrographs, regardless of the interpass temperature used, is that columnar grains are observed in the FZ, surrounded by austenite with different morphologies: intergranular austenite (AI), Widmanstätten austenite (AW), and allotriomorphic austenite (AA). Within the grains, intragranular and Widmanstätten austenite have been found. These morphological aspects of the resulting microstructure are clearly observed in Figure 4 (a)-(c). According to Ramirez et al.¹⁴, intragranular austenite is obtained due to the thicker grains formed in this region. The explanation follows the classical mechanism confirmed by previous results^{11,18-27}.

A larger grain size reduces the grain boundary area per volume and, therefore, less austenite will form from the ferrite at the grain boundaries during cooling. Therefore, the phase balance represented by their volume fractions and spatial distributions besides their morphological characteristics is mainly related to their specific grain boundary area and the local cooling rates. These main key parameters strongly relate to the growth kinetics of the phases developed during the welding procedures, which in turn, are defined by the welding parameters and the local thermophysical properties of the material^{11-16,18-27}. Consequently, larger regions in the center of the ferrite grains will be available for the nucleation

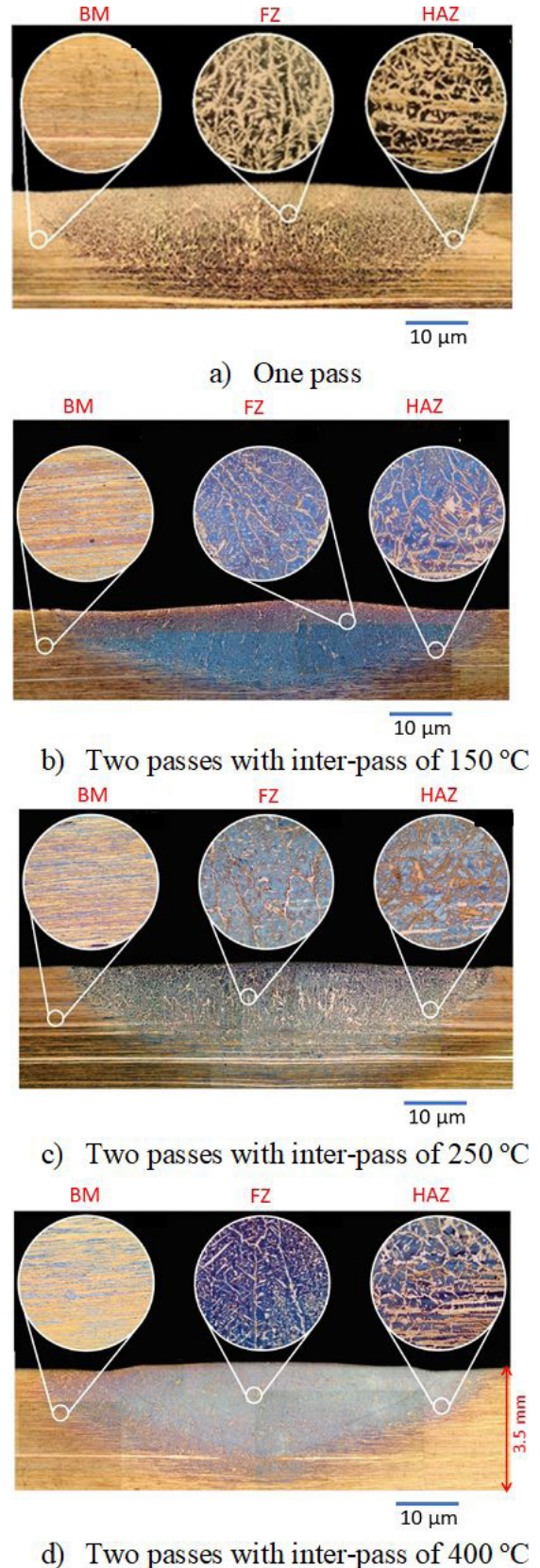


Figure 2. Microstructures of the stainless-steel tubes wall after TIG welding (Caption: BM – base metal; FZ – fusion zone; HAZ–heat affected zone).

and growth of austenite due to the resulting supersaturation with austenitizing elements of the ferrite phase. As a result, a higher thermodynamic potential is available for the intragranular precipitation in these supersaturated regions of ferrite. The mechanism of grain growth in these zones is

thermally activated. The final size and shape of the grains depend on the local thermal history. Thus, the final grain structure is achieved for a particular region of the joint following its own path. Therefore, the final grain spatial distribution is a function of the materials properties such

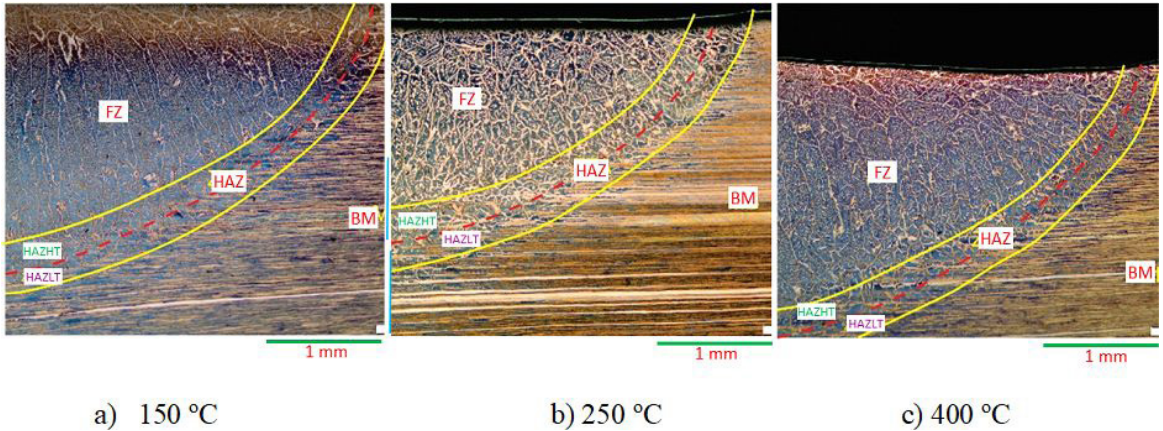


Figure 3. Transversal section of the weld region produced by TIG process with inter-passes temperatures: a) 150 °C, b) 250 °C, c) 400 °C, respectively. (Caption: BM – base metal; FZ- fusion zone; HAZ- heat affected zone, HAZHT- heat-affected zone of high temperature and HAZLT- heat-affected zone of low temperature).

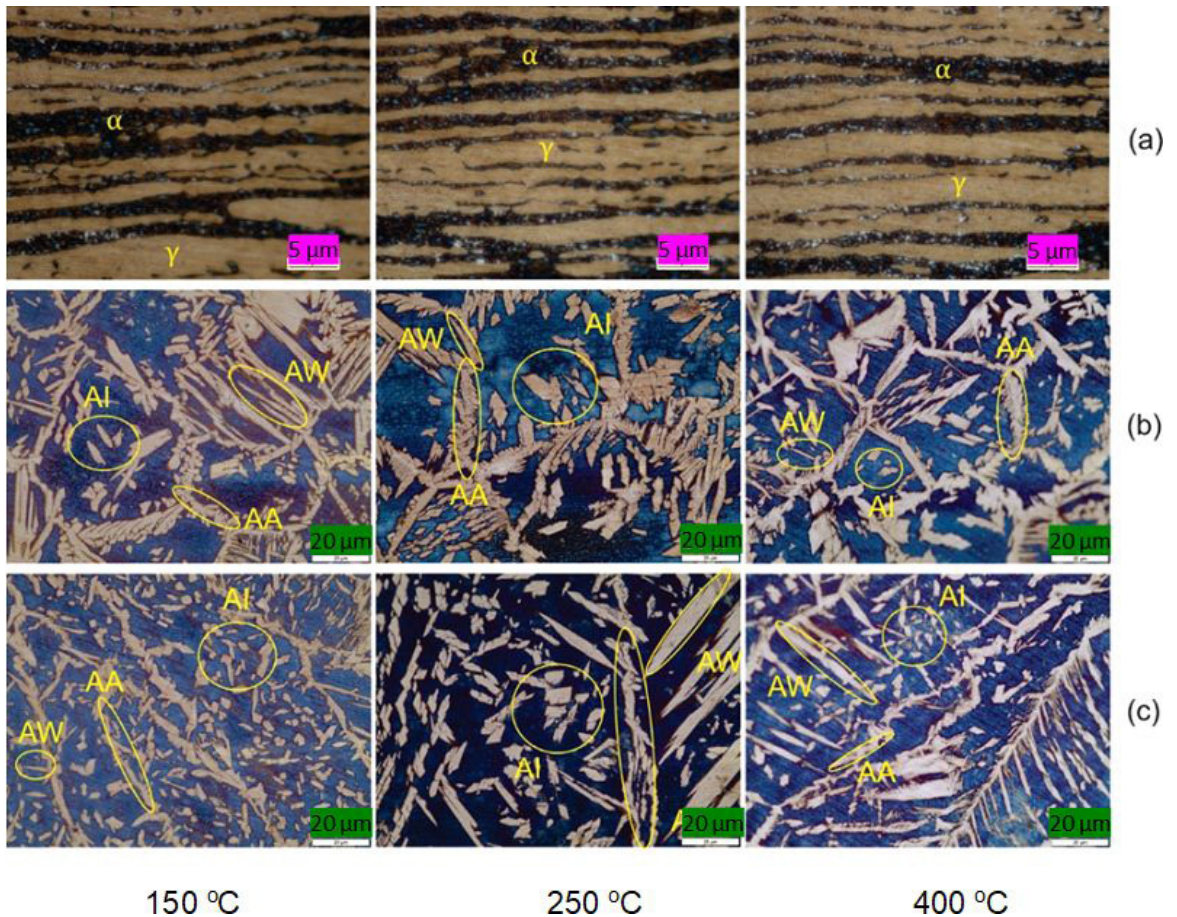


Figure 4. Morphology of the microstructures observed in the regions: (a) base metal BM, (b) heat affected zone HAZ, and (c) fusion zone FZ, with inter-passes temperatures of 150 °C, 250 °C, and 400°C, respectively. (Caption: AW - Widmanstätten austenite; AA - allotriomorphic austenite; AI - intragranular austenite).

as thermal conductivity, specific heat capacity, heat fusion, and heat input distribution²⁶⁻³⁰. Therefore, the grain size and phase volume fractions distribution are coupled phenomena affected by the volumetric heat source shape²⁵⁻²⁷, which are dynamically developed during the welding schedule designed to achieve balanced phases and hence welded joints with controlled properties, mainly its mechanical and corrosion resistance.

Comparing Figure 4 (a)-(c), the effects of inter-pass temperatures on the microstructure are clear. However, this discussion is only possible with an insight into the temperature pattern developed under such operational conditions. Figure 5 shows the recorded temperature during welding with programmed inter-pass temperatures of 150, 250, and 400 °C. The criterion for starting the second pass was achieved when the monitored positions' recorded temperatures were lower than the specified values, indicating that all welding beads cooled to a lower interpass specified value.

The phase's quantitative analysis was carried out using 20 images randomly selected for each welding zones assuming the classification presented in Figure 4. The quantitative phase analysis of the welded steel pipes of each region is listed in Table 3.

The FZ always presented a larger amount of ferrite than the HAZ, independently of the interpass temperature used. This result is attributed to a greater proportion of grain boundaries per volume when compared to the HAZ, as previously mentioned. The BM showed an average volumetric fraction of 48.33%±1.21% of ferrite and 51.67%±1.29 of austenite, which indicates a good balance between the phases. After the welding process had been carried out, the volume fraction of ferrite increased along with increasing interpass temperatures. According to the NORSOK M-601 standard¹², the fraction of ferrite in the welded region must be between 30 and 70%. The composition of none of the samples analyzed was outside of this safety region, as

Table 3. Quantitative phase analysis of the welded steel pipes with different interpass temperatures.

Inter-pass temperature	Region	Fraction of ferrite (%)	Fraction of austenite (%)
As received	BM	48.33±1.21	51.67±1.29
150 °C	FZ	53.52±1.34	46.48±1.16
150 °C	HAZ	48.52±1.22	51.48±1.29
250 °C	FZ	54.84±1.37	45.16±1.13
250 °C	HAZ	50.95±1.27	49.05±1.23
400 °C	FZ	56.84±1.42	43.16±1.08
400 °C	HAZ	52.51±1.31	47.49±1.18

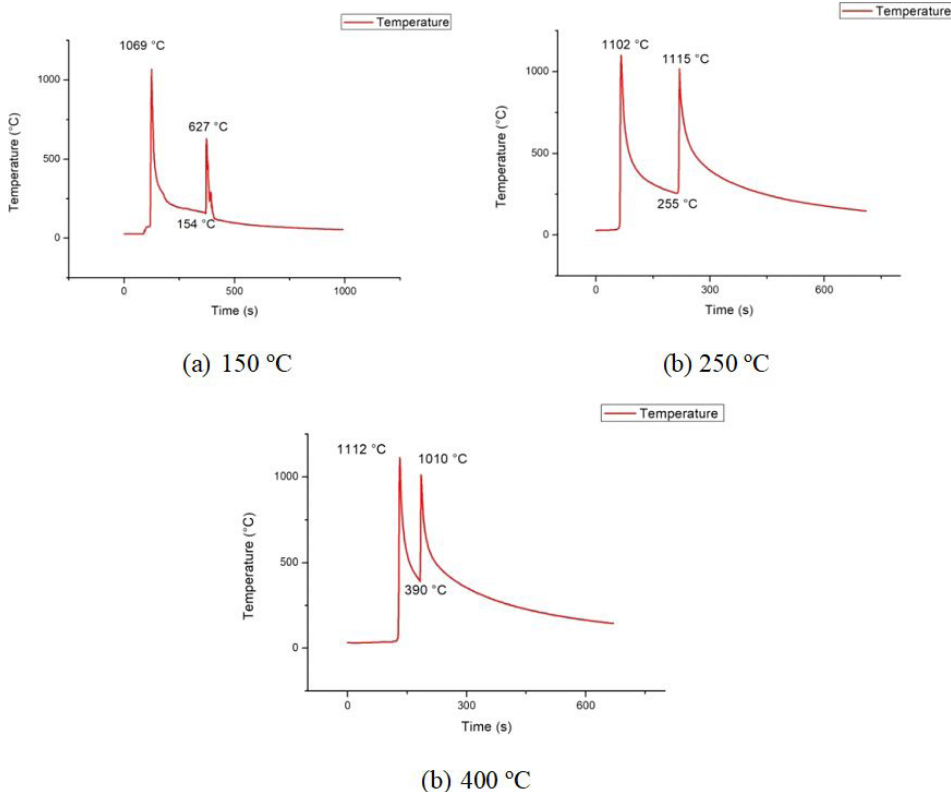


Figure 5. Thermal profiles indicating inter-pass temperatures and temperature evolutions during the welding procedures: a) 150 °C, b) 250 °C, and c) 400 °C.

established in the standard for all welding zones, indicating that, considering only this criterion, the welding procedures were successful. This is attributed to a greater cooling rate in the FZ and possible volatilization of alloy elements with a strong austenitizing effect, such as N, in the FZ. On the other hand, in the HAZ, the mechanism is explained by the local cooling rate and elemental diffusion, which is characteristic of the autogenous process.

The proportion of ferrite increased as the interpass temperature increased. The higher the interpass temperature, the smaller the temperature gradient and the cooling rate will decrease. In this way, the cooling rate in the material with an interpass temperature of 150 °C generates a larger temperature gradient and a higher cooling rate than observed for inter-pass temperatures of 250 °C and 400 °C, causing a refinement of the grains, as can be seen in Table 4.

Materials manufactured with columnar grains usually exhibit higher resistance in the longitudinal direction, as the grains are aligned in the maximum load direction. The decrease in grain boundaries that occurs when changing an equiaxed to a columnar structure also favors creep resistance, corrosion resistance, and tensile strength²⁰.

No evidence of significant deleterious phases was found in any analyzed regions using the combined analysis of OM, SEM, and X-ray diffraction. However a small amount of

secondary deleterious phases might be present, however undetected, because the analytical methods employed are sensible only for volume fractions higher than 2%^{11,23}. SEM micrographs produced with secondary electrons are shown in Figure 6. The images were obtained with a magnification of 10,000x, where the elements present in each phase were also quantified through energy dispersion spectroscopy (EDS). In none of these micrographs, it was possible to observe the evidence of the sigma phase (σ). The EDS analysis did not show significant changes in the distribution of the alloying elements for the FZ and HAZ zones, regardless of the interpass temperature. Still, the Cr in the ferrite phase was consistently higher than in the BM, as expected due to its effect as a stabilizer of the ferrite phase²⁶⁻³⁰. XRD analysis for the severest welding condition of this study is presented in Figure 7. As can be observed, small peaks of possible sigma phases were identified using Rietveld refinement.

Table 4. Quantitative analysis of the width of columnar grains in the fusion zone.

Interpass temperature	Columnar grains (μm)	Confidence level 95% (μm)
150 °C	48.87 \pm 1.20	1.13
250 °C	59.13 \pm 1.48	1.90
400 °C	61.83 \pm 1.55	5.52

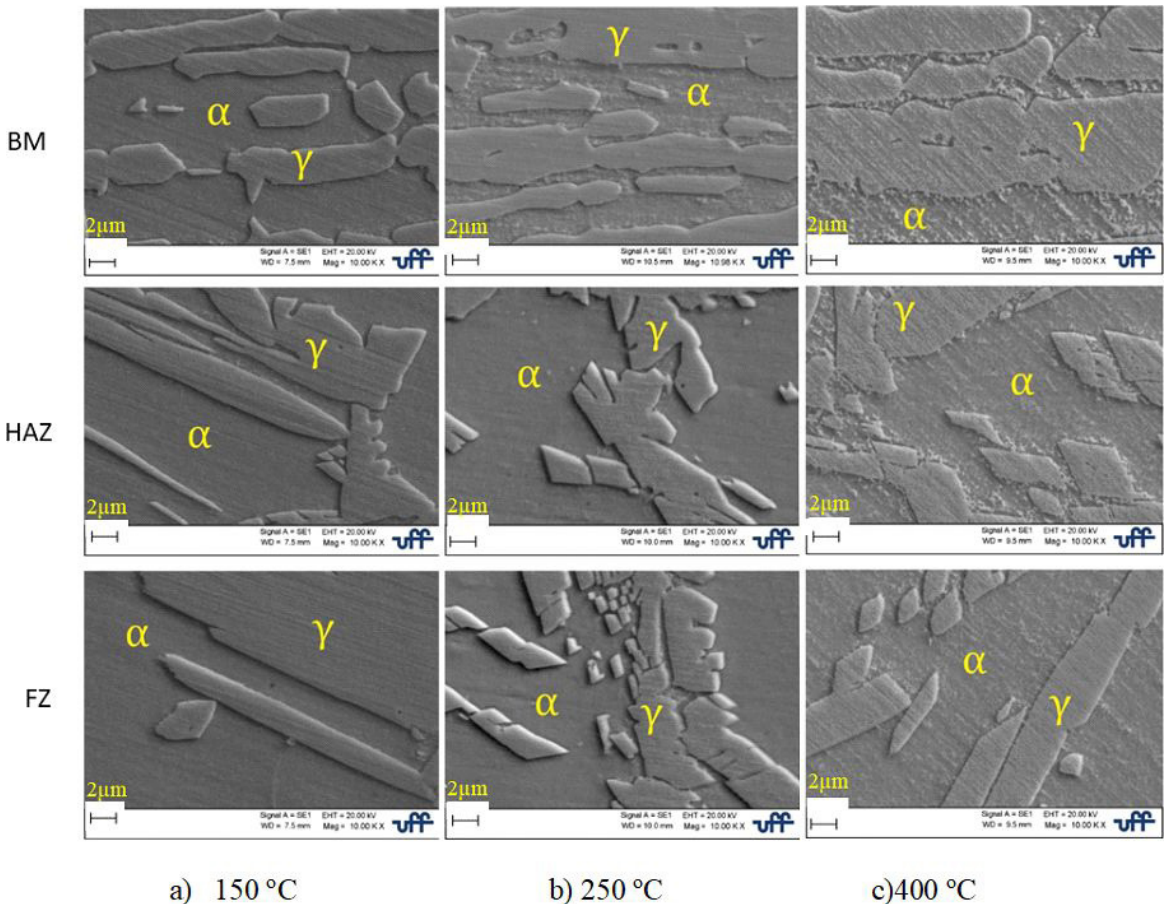


Figure 6. SEM micrographs of the BM, HAZ, and FZ regions (from top to bottom) of a stainless-steel tube welded with inter-pass temperatures: a) 150 °C, b) 250 °C, and c) 400 °C, respectively.

These results indicated that σ phase could be formed in a negligible amount undetectable with our analysis method. Thus, we used a simple relationship able to predict the σ phase volume fraction as a function of local cooling rates ($\Delta T/\Delta t$), Equation 1.

$$\sigma = 0.33 \times \left(\frac{\Delta T}{\Delta t} \right)^{-1.05} \quad (1)$$

This model has been applied by Castro et al.^{26,27}, where the authors propose a model capable of predicting the thermal history of a superduplex stainless steel and its mechanical properties developed after welding, adjusting the thermophysical parameters based on data measured in their work. Using Equation 1 for the cooling rates obtained from the thermocouples measurements, Table 5 was obtained. As observed, the predicted σ phase volume fractions would be very low and regarded as negligible, which would preserve the material's properties indicating that the designed interpass

temperatures could be implemented to the field practical process using the proposed parameters of this study.

3.2. Polarization curve

Before measuring the polarization curves, the open circuit potential was recorded for 30 min to stabilize the potential. The curves E (mV) $\times \log |i|$ (μA) were obtained for the samples representing the welding joint zones corresponding to the interpass temperatures of 150, 250, and 400 °C, respectively. The polarization curve is constructed starting from the stabilized open circuit potential and by scanning the potential and recording the current density for a fixed area exposed to corrosion solution, obtaining the measured data (E (mV) $\times I$ (μA)). The curve starts with a potential above the corrosion potential, and by varying the current density, the corrosion potential is obtained (E_{corr}). After reaching E_{corr} , the potential gradually increases, indicating the film's gradual passivation formed in the material surface^{11,15,23}. The position where the current increases suddenly are selected

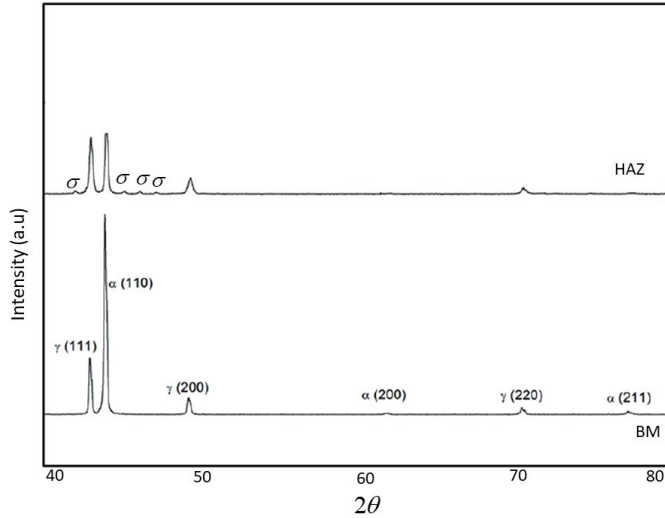


Figure 7. Comparison of the XRD pattern of HAZ with an interpass temperature of 400 °C with the base metal, BM.

Table 5. The sigma phase's maximum volume fraction and reformed austenite and the grain sizes predicted for welding conditions of this study^{26,27}.

Voltage (V)	Current (A)	Speed (mm.s ⁻¹)	Width bead (mm)	Thermal input (kJ.mm ⁻¹)	Ferrite grain size (μm)	Reformed austenite (%)	Maximum expected volume fraction of sigma phase (%) ^{20,21}
30	179	7.41±0.22	6.35±0.22	0.7	159±4	20.7±0.4	0.0006
30	178	4.33±0.13	6.35±0.22	1.2	175±5	27.5±0.8	0.0019
30	180	3.05±0.09	6.35±0.22	1.7	210±4	57.3±0.7	0.0269
25.7	170	6.76±0.20	8.00±0.22	0.5	73 (75*)	(36.2*)	0.0011
25.7	166	2.24±0.06	8.00±0.22	1.5	217±6 (232*)	42.5±0.9 (41.6*)	0.0026
25.7	169	1.59±0.04	8.00±0.22	2.2	344±8 (347*)	49.7±0.6 (48.2*)	0.0345
30	178	4.33±0.14	10.50±0.22	1.2	154±2	21.9±0.3	0.0013
30	179	4.33±0.13	6.35±0.22	1.2	174±3	27.2±0.5	0.0018
30	179	4.33±0.14	2.00±0.22	1.2	175±4	27.5±0.7	0.0055

* Mean of 10 random samples.

as the pitting potential (E_{pit}). The E_{pit} parameter indicates the material's resistance to corrosion by forming the initial pitting corrosion, that is, the lower the potential (E_{pit}), the lower the corrosion resistance of the material. The results obtained for the FZ and HAZ are shown in Figures 8 and 9, respectively. The results of FZ and HAZ are confronted with BM to identify possible deterioration in the corrosion properties of the welded joints^{11,15,28}.

Both FZ and HAZ regions exhibit pitting potentials in the same order as the BM (see Table 6). The results indicated that the FZ shows a slight decrease in the pitting potential for an interpass temperature of 400°C. Conversely, the HAZ pitting potential slightly increased with the interpass temperatures but higher than the reference BM. For both

FZ and HAZ zones, the observed effects were small. Thus, we considered that the resistance to pitting corrosion of the FZ and HAZ is not significantly differed from the BM regardless of the interpass temperature used in this study (see estimated statistical errors in Table 6).

3.3. Vickers hardness

Figure 10 shows the Vickers' hardness of samples measured in a transversal section for varying interpass temperatures. Analyzing the results, we identify that the Vickers' hardness error bars associated do not distinguish trends. Thus, we can assume that no deleterious effects on the welding joint's hardness are observed, independently of the interpass temperature used.

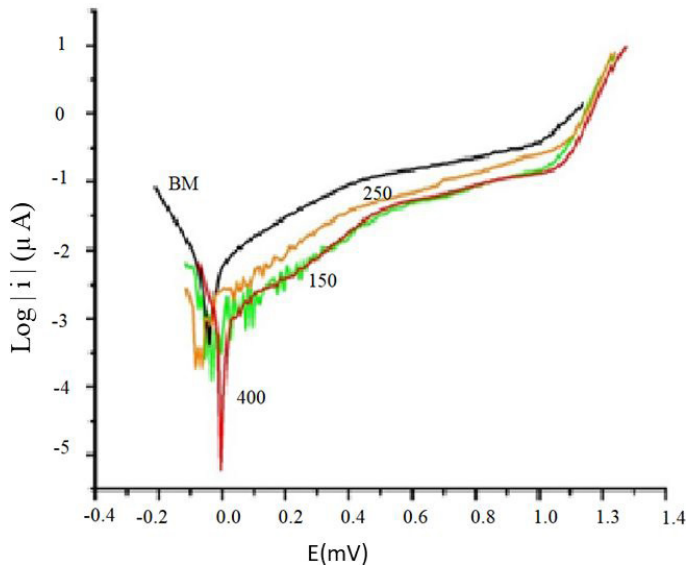


Figure 8. Comparison of polarization curves of the fusion zone (FZ) for different inter-pass temperatures (150 °C, 250 °C, and 400 °C), with the base metal as reference.

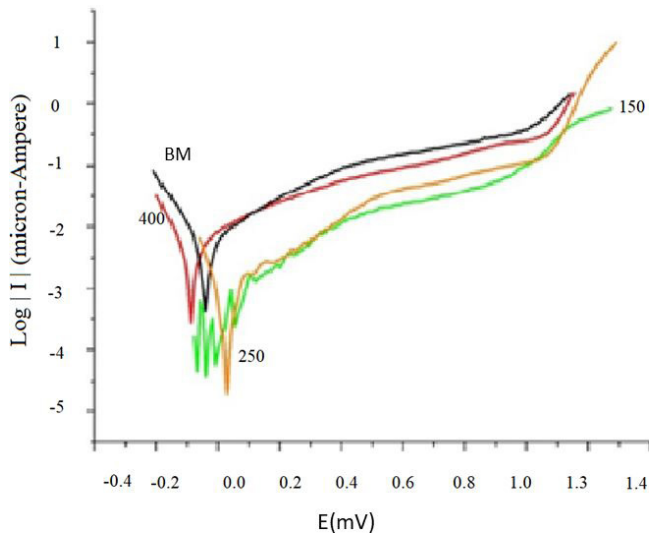
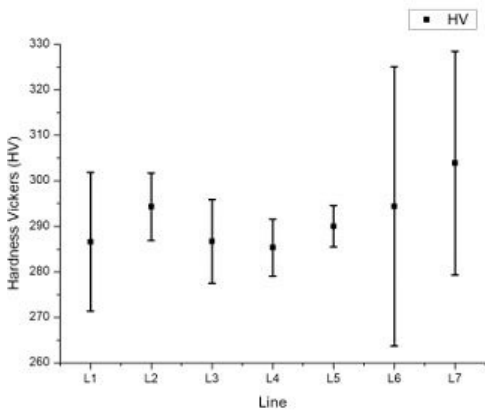
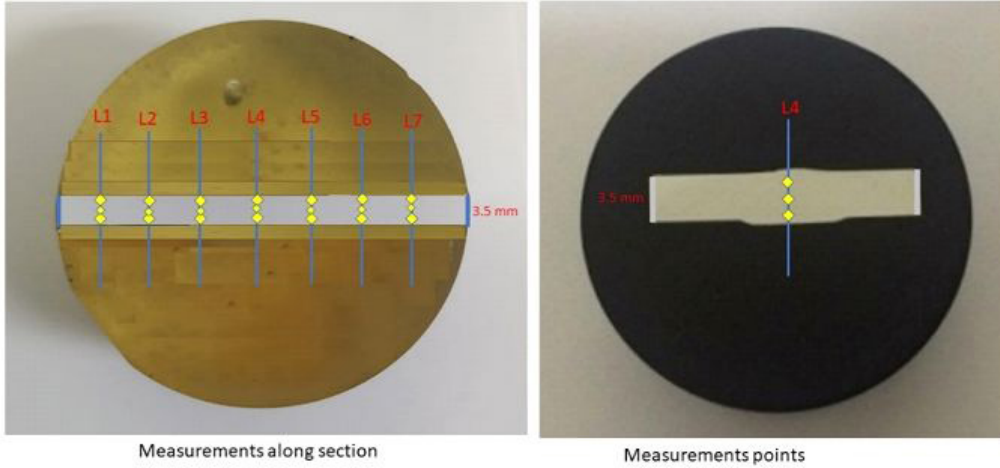


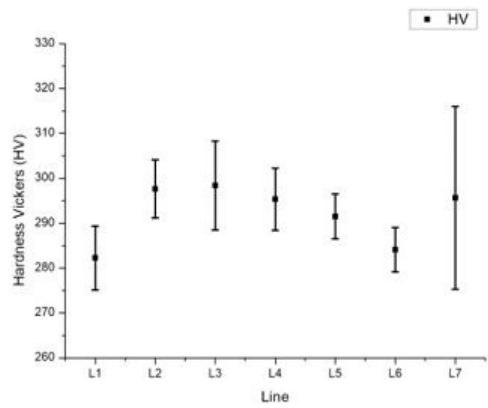
Figure 9. Comparative polarization curves of the heat-affected zone (HAZ) for different inter-pass temperatures (150 °C, 250 °C, and 400 °C), with the base metal as reference.

Table 6. Pitting potential, E_{pitt} (mV), for each inter-pass temperatur for the various welding zones.

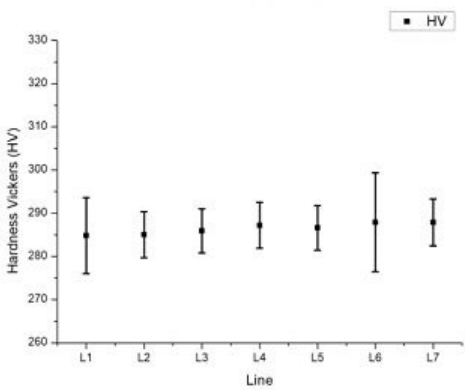
Inter-pass temperature	FZ	HAZ	BM
150 °C	1.0061±0.0251	1.0610±0.0265	1.0086±0.0252
250 °C	1.0871±0.0271	1.1018±0.0275	-
400 °C	0.8627±0.0216	1.0825±0.0271	-



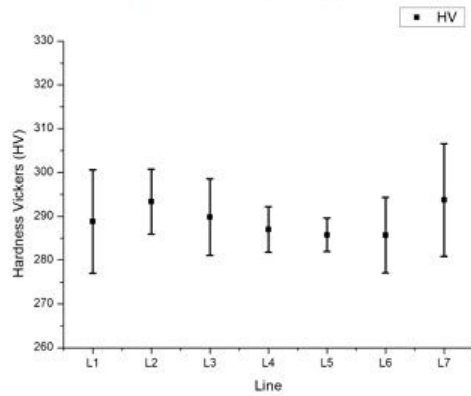
a) Single pass



b) 150 °C (two passes)



c) 250 °C (two passes)



d) 400 °C (two passes)

Figure 10. Hardness measurements along the transversal section of samples: (a) with single-pass, b) with interpass temperature at 150 °C; c) with interpass temperature at 250 °C, d) with interpass temperature at 400 °C.

4. Conclusions

The multiple pass welding of the superduplex stainless steel SAF-2507 SDSS is a complex and technologically important issue. In this work, the influence of interpass temperatures of 150, 250, and 400 °C was investigated in respect to microstructure, hardness and corrosion resistance of the welds. Regardless of the interpass temperature, a suitable ferrite/austenite balance for FZ and HAZ was maintained, besides that hardness and corrosion resistance were not significantly affected. Moreover, microstructural analysis confirmed that the presence of the deleterious sigma phase was negligible. Although the pitting corrosion experiments indicated a small decrease as the interpass temperatures were increased, the standard requirements for a suitable welding process were attained. Based on the combined results of phase volume fractions, microstructural evolution, and pitting corrosion parameters of the FZ and HAZ compared with the BM, we conclude that the possibility of the two pass welding process with temperatures varying from 150 to 400°C is viable. However, additional investigations are necessary depending on the welding schedule.

5. Acknowledgments

The authors acknowledge CAPES. C. Santos thanks FAPERJ (grants E-26/202.997/2017) and CNPq (311119/2017-4), J.A. Castro thanks FAPERJ (E-26/202.888/2018 grant: 239505) and CNPq (302534/2019-9) for the financial support.

6. References

- Hosseini VA, Wessman S, Hurtig K, Karlsson L. Nitrogen loss and effects on microstructure in multipass TIG welding of a super duplex stainless steel. *Mater Des.* 2016;98:88-97.
- Souza JPB, Arias AG, Pardal JM, Mainier FB, Ferreira MLR, Tavares SM. Análise da resistência à corrosão por pite em soldas de reparo pelo processo TIG em aço inoxidável superduplex UNS S32750. *Soldag Insp.* 2011;16(2):104-13.
- Sandvik Materials Technology. [homepage on the Internet]. Suécia: Sandvik Materials Technology; 2018 [cited 2020 June 1]. Available from: <https://www.materials.sandvik/en/products/tube-pipe-fittings-and-flanges/highperformance-materials/duplex-stainless-steel/sandvik-saf-2507/>
- Reick W, Pohl M, Padilha AF. O desenvolvimento dos aços inoxidáveis ferríticos-austeníticos com microestrutura duplex. In: 47th ABM Annual Congress; 1992; Belo Horizonte. Proceedings. São Paulo: ABM; 1992.
- Kumar R, Bharathi S. A review study on A-TIG Welding of 316(L) austenitic stainless steel. *International Journal of Emerging Trends in Science and Techn.* 2015;2(3):2066-72.
- Caetano GQ, Silva CC, Motta MF, Miranda HC, Farias JP, Bergmann LA, et al. Intergranular corrosion evaluation of friction stir welded AISI 410S ferritic stainless steel. *J. Mater. Res. Technol.* 2019;8(2):1878-87.
- Chauhan A, Samad A, Mathur YB. Experimental study on autogenous TIG welding of mild steel material using lathe machine. *International Journal on Future Revolution in Computer Science & Commun Eng.* 2017;3(9):172-80.
- Jurica M, Kožuh Z, Garašić I, Bušić M. Optimization of the A-TIG welding for stainless steels. *IOP Conf. Series: Materials Science and Engineering.* 2018;329:012012.
- Kumar H, Singh NK. Performance of activated TIG welding in 304 austenitic stainless steel welds, ICEMS 2016. *Materials Today: Proceedings.* 2017;4:9914-8.
- Vasconcellos PIG, Rosenthal R, Paranhos RPR. Study of the welding of duplex and superduplex stainless steel pipes in the 5G Position. *Soldag Insp.* 2010;15(3):191-9.
- Fonseca GS, Barbosa LOR, Ferreira EA, Xavier CR, Castro JA. Microstructural, mechanical, and electrochemical analysis of duplex and superduplex stainless steels welded with the autogenous TIG process using different heat input. *Metals (Basel).* 2017;7:538-48.
- Hammood AS, Noor AF, Alkhafagy MT. Evaluation of corrosion behavior in artificial saliva of 2507 and 2205 duplex stainless steel for orthodontic wires before and after heat treatment. *J Mater Sci Mater Med.* 2017;28:187-98.
- Standards Norway. NORSOK Standard M-601: welding and inspection of piping. Norway: Standards Norway; 2016.
- Ramirez AC, Lippold J, Brandi SD. The relationship between chromium nitride and secondary austenite precipitation in duplex stainless steels. *Metall Mater Trans, A Phys Metall Mater Sci.* 2003;34:1575-97.
- Verma J, Taiwade RV. Review effect of welding processes and conditions on the microstructure, mechanical properties and corrosion resistance of duplex stainless steel weldments - A review. *J Manuf Process.* 2017;25:134-52.
- Xavier CR, Delgado HG Jr, Castro JA. An Experimental and numerical approach for the welding effects on the duplex stainless steel microstructure. *Mater Res.* 2015;18(3):489-502. <http://dx.doi.org/10.1590/1516-1439.302014>.
- ASTM International. ASTM E-562-19. Standard Test Method for Determining Volume Fraction by Systematic Manual Point Count. West Conshohocken: ASTM International. <http://dx.doi.org/10.1520/E0562-19>.
- Bracarense AQ. Processo de Soldagem TIG - GTAW. Belo Horizonte: ESAB; 2000.
- Gomes, DA, Castro, JA, Xavier, CR, Lima, CAC. Analysis of Residual Stress by the Hole-Drilling Method and Hardness in Dissimilar Joints of Austenitic Stainless Steel AISI 316L and Inconel 718 Alloy by Autogenous GTAW Process. *Materials Research,* 2019;22(Suppl. 1):e20180844. <http://dx.doi.org/10.1590/1980-5373-mr-2018-0844>.
- Alves FP. Estudo da evolução microestrutural de juntas de aços inoxidável superduplex em soldagem TIG orbital com múltiplos passes [dissertação]. Rio de Janeiro: Universidade Federal do Rio de Janeiro; 2011.
- Xavier CR, Delgado HG Jr, Castro JA. An experimental and numerical approach for the welding effects on the duplex stainless steel microstructure. *Mater Res.* 2015;18(3):489-502. <http://dx.doi.org/10.1590/1516-1439.302014>.
- Xavier CR, Delgado JHG, Castro JA, Ferreira AF. Numerical predictions for the thermal history, microstructure and hardness distributions at the HAZ during welding of low alloy steels. *Mater Res.* 2016;19:520-33.
- Fonseca GS, Oliveira PM, Diniz MG, Bubnoff DM, Castro JA. Sigma phase in superduplex stainless steel: formation, kinetics and microstructural path. *Mater Res.* 2017;20:249-55.
- Sieurin H, Sandström R. Sigma phase precipitation in duplex stainless steel 2205. *Mater Sci Eng A.* 2007;444:271-6.
- Xavier CR, Campos MF, Castro JA. Numerical method applied to duplex stainless steel. *Ironmak Steelmak.* 2013;40:420-9.
- Castro JA, Fonseca GS, Almeida D, Rolim LC, Xavier CR, Olivera EM. Effects of heat input conditions on the local thermophysical properties of super duplex stainless steels. *Mater Sci Forum.* 2018;930:317-21.
- Castro, JA, Oliveira, EM, Almeida, DSS, Fonseca, GS, Xavier, CR. Effects of local heat input conditions on the thermophysical properties of Super Duplex Stainless Steels (SDSS). *Materials Research.* 2018;20(Suppl. 1):153-61. <http://dx.doi.org/10.1590/1980-5373-mr-2017-0384>.
- Zhu M, Zhang Q, Yuan Y, Guo S, Huang Y. Study on the correlation between passive film and AC corrosion behavior of 2507 super duplex stainless steel in simulated marine

- environment. *J Electroanal Chem.* 2020;864:114072. <http://dx.doi.org/10.1016/j.jelechem.2020.114072>.
29. Ogawa K, Osuki T. Modelling of sigma phase precipitation in super duplex stainless steel weld metal. *ISIJ Int.* 2020;60(5):1016-21. <http://dx.doi.org/10.2355/isijinternational.ISIJINT-2019-537>.
30. Zhang Z, Zhang H, Hu J, Qi X, Bian Y, Shen A, et al. Microstructure evolution and mechanical properties briefly heat-treated SAF 2507 Super Duplex Stainless Steels welds. *Constr Build Mater.* 2018;168:358-345. <http://dx.doi.org/10.1016/j.conbuildmat.2018.02.143>.